Results in Chemistry 30 (2026) 103854

Contents lists available at ScienceDirect

Results in Chemistry

journal homepage: www.sciencedirect.com/journal/results-in-chemistry

Comparative density functional theory study on the band gap, effective mass and optical properties of graphene monolayer on SiC(0001) substrate

Elaheh Mohebbi [a], Pierluigi Stipa [a], Eleonora Pavoni [a], Marina Petroselli [a], Luca Pierantoni [b], Emiliano Laudadio [a,*], Davide Mencarelli [b]

[a] Department of Science and Engineering of Matter, Environment and Urban Planning (SIMAU), Marche Polytechnic University, 60131 Ancona, Italy
[b] Information Engineering Department, Marche Polytechnic University, 60131 Ancona, Italy

ARTICLE INFO

Keywords:
DFT calculation
Graphene
Effective mass
THz frequency
Electronic and optical properties

ABSTRACT

The semiconductor characteristic has never been shown, despite the fact that various Density Functional Theory (DFT) approaches have been applied to ascertain the electronic band structure of the graphene monolayer (GML) over the Si-terminated SiC surface. In this study, using an accurate Meta Generalized Gradient Approximation (MGGA) functional, the results showed that the GML@SiC (0001) exhibits a straight band gap of 0.57 eV along the K → K in the reciprocal space, while Generalized Gradient Approximation (GGA) and HSE06 (Heyd-Scuseria-Ernzerhof) hybrid functionals anticipated the metallic properties of GML. Different functionals display distinct electronic trends is due to how they mathematically treat electron self-interaction, orbital inhomogeneity via kinetic energy density τ (r) and nonlocal screening at a heterogeneous 2D(GML)/3D(SiC) interface. More, the lower estimated effective mass (m^*) of electrons in GML calculated by GGA and HSE06 functionals with respect to MGGA, suggests minor interaction between photon-charge carriers of GML with the substrate. While the results corresponded to Im (ω) part of dielectric constants showed the presence of the first optical peak at 36–48 THz using different functionals, the high Re(ω) value of 28.03 has been calculated for GML@SiC(0001) by MGGA functional. Since Graphene GML@SiC (0001) is a premier platform for wafer-scale electronic devices, its main uses include high-frequency electronics, quantum metrology standards, and environmental sensing, and for this reason, the present study would help to utilize the graphene-based heterostructures for enabling advanced, tunable, and efficient optoelectronic devices.

1. Introduction

The fabrication of graphene-based electronic devices is thought to be feasible through the growth of epitaxial graphene on silicon carbide (SiC). As a result, great effort has been made in recent years to characterize this material and enhance its development and features. Hexagonal single-crystal SiC (6H-SiC) is typically utilized for graphene formation. The SiC (0001) surfaces are suitable for growing graphene. The Si-terminated (0001) and C-terminated (0001) faces are present on these surfaces [1,2]. The characteristics of graphene produced on different faces are varied. The Si-face is a superior option for producing uniform, controllable monolayer to few-layer graphene over large areas compared to the C-face [3]. The existence of a graphene buffer layer (GBL) is another characteristic of graphene produced on the Si-face. The GBL is a carbon layer with a honeycomb structure, but some of the carbon atoms are displaced out of plane. The atomic structure of the GBL is a periodic pentagon/heptagon arrangement in the $6\sqrt{3} \times 6\sqrt{3}R30$ honeycomb superstructure, which was revealed by detailed Scanning Tunneling Microscopy (STM) observation [4,5].

Graphene as a well-known material, is a single-atom-thick two-dimensional (2D) honeycomb lattice of carbon atoms. It exhibits exceptional mechanical strength, ultra-high electrical and thermal conductivity, and optical transparency [6–8], spurring extensive research into its variants and commercial applications including energy storage [9], electronics and optoelectronics [10,11], sensing [12–14], biomedicals [15–18] and catalysts [19–21]. Since graphene has no band gap, several researchers have been focused on the structural manipulation of the graphene to introduce a gap [22–24]. Interaction of graphene sheet with the SiC(0001) substrate naturally creates a band gap in the first layers by covalent bonding (GBL) or symmetry-breaking

* Corresponding author.
E-mail addresses: e.mohebbi@staff.univpm.it (E. Mohebbi), p.stipa@staff.univpm.it (P. Stipa), e.pavoni@staff.univpm.it (E. Pavoni), m.petroselli@pm.univpm.it (M. Petroselli), l.pierantoni@staff.univpm.it (L. Pierantoni), e.laudadio@staff.univpm.it (E. Laudadio), d.mencarelli@staff.univpm.it (D. Mencarelli).

https://doi.org/10.1016/j.rechem.2026.103854
Received 3 March 2026; Accepted 12 September 2026
Available online 13 September 2026
2211-7156/© 2026 The Authors. Published by Elsevier B.V. This is an open access article under the CC BY-NC-ND license (http://creativecommons.org/licenses/by-nc-nd/4.0/).

interactions when another graphene monolayer (GML) is added on top of GBL in the interface. According to different theoretical and experimental studies, GBL is a semiconductor by nature. It is covalently bound to about one-third of the silicon atoms in the substrate, breaking the honeycomb symmetry and creating a large band gap that has been measured to be more than 0.5 eV, both computationally and experimentally [25,26]. The linear Dirac cone is restored when GML decouples from the substrate, and according to many research finding, GML has a narrower substrate-induced band gap than GBL. Zhou et al. [27] revealed that when graphene is epitaxially grown on SiC substrate, a gap of ≈0.26 eV is produced. This gap decreases as the sample thickness increases and eventually approaches zero when the number of layers exceeds four. An experimental study of Coletti et al. [28] has reported F4-TCNQ acts as a strong dopant on graphene/SiC, inducing a small and tunable band gap. In bilayer graphene, adsorption of F4-TCNQ can open a band gap of approximately 0.25–0.31 eV, depending on molecular concentration and external fields. It effectively transforms graphene into a semiconducting material by creating a charge transfer, typically 0.45*e* per molecule, and increasing the band gap to more than double its initial value in bilayer systems. Moreover, experimental high-resolution angle-resolved photoemission spectroscopy (ARPES) measurements done by Sugawara et al. [29] showed that the band gap gradually enhanced from 0.25 eV in the pristine sample (graphene on SiC(0001)) to 0.5 eV upon hydrogen exposure, as seen in the energy distribution curve at the *K*-point.

Regarding to theoretical studies, an ab initio study performed by Peng et al. [30] has revealed that no band gap has found in the Dirac bands in a defect-free graphene is grown on SiC substrate, using Generalized Gradient Approximation (GGA)/PBE functional. Indeed, they introduced a finite density of Stone-Wales defects in the graphene layer(s) and then observed that a gap is opened and decreases as the thickness of the graphene layers increases. Furthermore, Mattausch et al. [31] using Local-density approximations (LDA) has predicted a metallic interface of GML on Si-terminated SiC (0001), while single or double graphene coverage on C-face is semiconducting or semi-metallic. A Density Functional Theory (DFT) study using Perdew–Burke–Ernzerhof (PBE) by Cavallucci et al., [32] has revealed that van der Waals (vdW) interactions stabilize opposite corrugation and rippling patterns in monolayer graphene on SiC. Low temperatures favor a state tracking the buffer layer topography, while external environmental factors can drive switching between multistable corrugation states. More, adsorption of NO_2 on monolayer epitaxial graphene on SiC (0001) has considered with PBE functional in an ab initio study with Caffrey et al. [33]. The results showed that GML on a SiC substrate has a surface work function increase of about 0.9 eV due to charge transfer from the underlying interface. A bilayer of graphene screens this charge, causing a smaller work function change and lower surface sensitivity. According to Kopylov et al. [34], and Mattausch et al. [35], the charge density difference (CDD)and charge transfer analysis for a GML on SiC substrate reveals strong interfacial covalent bonding and local sp^3 hybridization at the GBL interface, causing significant net charge transfer and *n*-type doping of the overlying graphene. In the first-principles study of Liu et al. [36], the results reveal that high electron localization function (ELF) values appear between the carbon atoms of the GBL and the surface silicon atoms of the SiC}(0001) substrate. Also, the localized electron distribution confirms strong covalent sp^3-like bonding interactions pinning the GBL to the substrate.

Although considerable progress has been made in modeling of graphene/SiC heterostructures, prior investigations typically rely on a conventional functional like PBE and LDA without quantifying how using other method selection like MGGA, HSE06 or GW shifts bandgap predictions, charge transfer, or dielectric functions. This lack of a unified benchmark creates uncertainty when comparing literature results. Motivated by this gap, the present study provides a systematic comparative evaluation across multiple DFT functionals, establishing clear guidelines for the reliable modeling of graphene/SiC optoelectronic devices. Moreover, previous ab initio calculations have demonstrated that the electronic bands of a single GML above the GBL are gapless and remarkably similar to the bands of a freestanding graphene layer when the SiC (0001) substrate is present. The band gap opening seen in the experimental measurements of Zhou et al. [27] and Sugawara et al. [29] has yet to be explained. In this study, we investigated how using a different approach can provide a band gap with the semiconductor property of GML over the SiC (0001) substrate that is comparable to the experimental one. Following our earlier work, we assessed the electronic and optical characteristics of GBL on SiC (0001) using the Meta-Generalized Gradient Approximation (MGGA) functional with various basis sets. We revealed that the MGGA-Medium functional can reproduce an indirect/direct band gap 0.65 eV/0.80 eV [26] in good agreement with the experimental band gap of this interface (> 0.5 eV) [25]. The GML on SiC surface are versatile material with several key applications like quantum metrology [37], spintronics [38], gas and biosensors, optoelectronics and photonics [39–41] and nanomedicine.

In order to complete our previous studies [26,42–44], this DFT study's primary objective is to determine whether the GML@SiC (0001) system, a graphene-based nanostructure, can amplify THz waves at low frequencies in the THz range. In order to achieve this, we evaluated the important characteristics of this heterostructure, including its electronic band structure, partial density of states (PDOS), effective mass (m^*), and several optical characteristics. It is important to note that the development of this crucial THz frequency technology in the future will require the use of innovative 2D graphene materials for plasmonic amplification of THz sources. In this DFT work for the first time, we demonstrated that a semiconducting feature of GML on SiC(0001) can reproduced using improved MGGA method, in which GML exhibits a direct band gap.

2. Methods

The DFT results were performed by using the Quantum ATK (QATK) [45] code. The Kohn–Sham (KS) formulation [46–48] has been answered by the linear combinations of atomic orbitals (LCAO) basis set [49]. To determine the electronic structure within DFT of GML on SiC (0001) substrate, we employed three distinct approaches: GGA/PBE (Generalized Gradient Approximation) [50], MGGA/TB09 [51], and HSE06 (Heyd-Scuseria-Ernzerhof) [52]. we decided to use all the three approaches to compensate for the theoretical gaps of each and obtain accurate predictions by exploiting the methods in synergy with each other and in comparison, to experimental measurements [53].

The GGA, MGGA, and HSE06 functionals represent progressively higher rungs on Jacob's ladder of density functionals [54]. They differ significantly in computational cost and how they address the severe underestimation of semiconductor band gaps due to self-interaction errors. GGA/PBE calculations rely only on electron density $\rho(r)$ and its gradient $\nabla\rho(r)$. This functional models the interaction of an electron with the average density of all electrons, it includes an unphysical interaction of an electron with itself [55]. Therefore, it suffers from a strong self-interaction error, severely underestimating band gaps or failing to capture localized defect states in graphene-based nanostructures [56,57]. MGGA/TB09 indeed depends on $\rho(r)$, $\nabla\rho(r)$, and additionally the Kohn-Sham kinetic energy density $\tau(r)$. It improves orbital and local potential descriptions over GGA [58]. TB09 models the exchange-correlation (ec) potential directly rather than deriving it as the derivative of an energy functional. This mimics the behavior of a discontinuity in the potential, leading to band gaps that rival expensive hybrid functionals or GW calculations. The inclusion of $\tau(r)$ allows the functional to distinguish between regions of single orbital dominance (like covalent bonds) and regions of overlapping densities (like electron gases). This yields a much more realistic spatial distribution of the local potential [54,59]. HSE06 as a screened hybrid functional that replaces a fraction (typically 25%) of the GGA exchange energy with nonlocal exact Hartree-Fock exchange split into short-range and long-range components. It fixes major self-interaction issues and yields more

accurate fundamental band gaps, however, demands high computing power [60,61].

In order to solve the shortcomings in the PBE functional and account for VdWs forces—which are essential for precise predictions of intermolecular interactions and structural properties—we used the Grimme dispersion correction for interface optimization [62]. This decision was based on the findings of our earlier paper, in which we searched for the most effective method of calculation for describing the covalent and noncovalent interactions between the GBL on SiC (0001) [26]. Since the functional's effectiveness and accuracy in capturing the subtleties of the electronic structure are strongly impacted by the basis set selection [50,51], we used the completely relativistic basis set of Ultra that is accessible for every element, as well as PseudoDojo pseudopotentials. We point out that there are more pseudo-atomic orbitals in this basis set. Additionally, all electron core treatment, a global orbital cut-off of 6 Å and Fermi orbital occupancy (no thermal smearing) were used. Full geometry optimization and calculation of electronic parameters were performed until the residual forces fell below 0.001 eV/A°. The electronic convergence tolerance was set to 10^{-5} eV. For all calculations, a kinetic energy cutoff of 110 Ry was chosen for the integration mesh.

Molecular projected self-consistent Hamiltonian (MPSH) computations were performed to analyse the energy levels of HOMO-LUMO of various geometries. MPSH calculations for a material system such as a 2D/3D heterostructure interfaces, acts as a powerful diagnostic tool to investigate how the localized molecular orbitals or sub-layer states are renormalized and shifted due to molecule-substrate or layer-layer interactions. The effective mass (m^*) calculations are performed by numerically evaluating the second-order derivative of the energy eigenvalues $E(k)$ with respect to the wave vector (k) near band extrema, yielding the effective mass tensor. Computations use finite-difference stencil methods on a localized grid around specified high-symmetry k-points.

The m^* of the carriers in graphene is calculated the energy-momentum relation [63]:

$$m^* = \frac{E(k)}{v_F^2} = \frac{\hbar k}{v_F} \tag{1}$$

where $E(k)$ refers to the band dispersion energy with effective velocity of $v_F \cong 10^6\ m/s$.

Then, the optical properties have been calculated. The real part of the dielectric function ($Re(\omega)$) relates to the material's refractive index (n), while its imaginary part ($Im(\omega)$) relates to the extinction coefficient (κ), also known as the absorption coefficient, and together these form the complex n calculated by the following Formula [61,64–66],

$$n = \sqrt{\frac{\sqrt{Re(\omega)^2 + Im(\omega)^2} + Re(\omega)}{2}} \tag{2}$$

$$\kappa = \sqrt{\frac{\sqrt{Re(\omega)^2 + Im(\omega)^2} - Re(\omega)}{2}} \tag{3}$$

The imaginary part of the n (defined also as the κ) is related to the absorption term of electromagnetic waves as they travel through a material.

Additionally, the term n is related to the complex relative permittivity (ϵ_r) are connected by,

$$n + i\kappa = \sqrt{\epsilon_r} \tag{4}$$

The linear response approach (Kubo formula) in the optical spectrum analyser is commonly used in QATK to compute optical conductivity $\sigma(\omega)$. $Re(\omega)$) and $Im(\omega)$) components are included in the complex tensor ($3 \times 3 \times N$) that represents the conductivity as a function of energy (frequency). It is possible to calculate the overall electronic and ionic contributions in addition to certain tensor components (xx, yy, zz). The frequency-dependent dielectric susceptibility $\chi(\omega)$ and conductivity are related by the following rule:

$$\sigma(\omega) = -i(\omega)\epsilon_r\chi(\omega) \tag{5}$$

3. Results and discussion

As described in our earlier study [26], the geometry of SiC(0001) surface was reproduced from experimental data [67,68]. We investigated the electronic structure and optical characteristics of GML@GBL@SiC(0001) using different approaches, utilizing the relaxed geometry derived from GGA functional. As shown in Fig. 1, the form and characteristics of the carbon sheets that resulted from optimizing the supercell on 6H-SiC(0001) consist of the first carbon layer, known as GBL, partially bonded to the substrate, kept a significant number of sp^2 hybridized sites. The second carbon sheet is corresponded to GML with hybrid sp^3-sp^2 hybridization which is typical for pure aromatic extended systems [69,70]. The C—C bond length between GBL and GML has shifted from 3.30 Å to a medium range of 3.49 Å and a maximum vertical length of 3.71 Å, according to the structural optimization calculations.

In the next step, using three different methodologies of GGA, MGGA, and HSE06 functionals, the band structures and PDOS computations of GML on the SiC (0001) surface are shown in Fig. 2**.** According to the DFT results, the metallic properties of GML with zero band gap were predicted by GGA and HSE06, whereas MGGA calculated a direct band gap of 0.57 eV along the K → K (K-points: 0.33, 0.33, 0.00) with valence energy level (VEL) of –0.12 eV and conduction energy level (CEL) of 0.45 eV. However, the results show that band structures corresponding to GGA and HSE06 are apparently similar, and only the energy level of the band index has a different value. According to MGGA calculations, the density of states near the Fermi level (the top of the valence band and the bottom of the conduction band) is primarily due to the contribution from carbon atoms (Fig. 3), whereas the substantial contributions of Si atoms below/after the Fermi energy was predicted by GGA/HSE06 calculations, respectively. According to the detailed experimental measurements reported by Zhou et al. [27], Sugawara et al. [29] and Coletti et al. [28], demonstrated that when GML is epitaxially grown on a 6H-SiC substrate, the bandgap of ≈ 0.25–31 eV is formed. Table 1 show the electronic band gap of GML@ SiC(0001) surface calculated with different functionals in our study, has compared to other experimental and theoretical studies. In this DFT study, for the first time, we were able to show the semiconductor property of GML@SiC(0001) resulting from a direct band gap derived with MGGA functional, although the theory value upper estimate the experimental data. In accordance with the other earlier calculations utilizing LDA or GGA approaches [30,31], the atomistic simulations have thus far indicated no bandgap for the defect-free GML on SiC.

The reasons why the GGA, MGGA, and HSE06 functionals show these specific electronic trends at the GML/SiC interface are directly addressed to the physics of self-interaction error, orbital kinetic energy density τ(r), and dielectric screening at a heterogeneous 2D(graphene)/3D(SiC) interface. Regarding to the metallic property predicted with GGA/PBE, at a heterogeneous interface like graphene/SiC, PBE over-delocalizes the electronic states across the interface. This artificial electron delocalization closes the subtle, substrate-induced band gap of graphene, leading to an incorrect prediction of purely metallic behavior. About semiconductor feature of this system obtained by the MGGA, this functional is highly sensitive to local density gradients. The mathematical ingredient of kinetic energy density τ(r) allows the functional to recognize variations in electron localization topologies e.g., distinguishing between covalent, metallic, and weak van der Waals regions. By accurately capturing these local gradients at the 2D/3D interface, the MGGA functional partially mitigates self-interaction errors and successfully resolves the symmetry-breaking effects induced by the SiC substrate, thereby correctly opening the small electronic band gap. On the other hand, while HSE06 typically corrects bulk semiconductor band

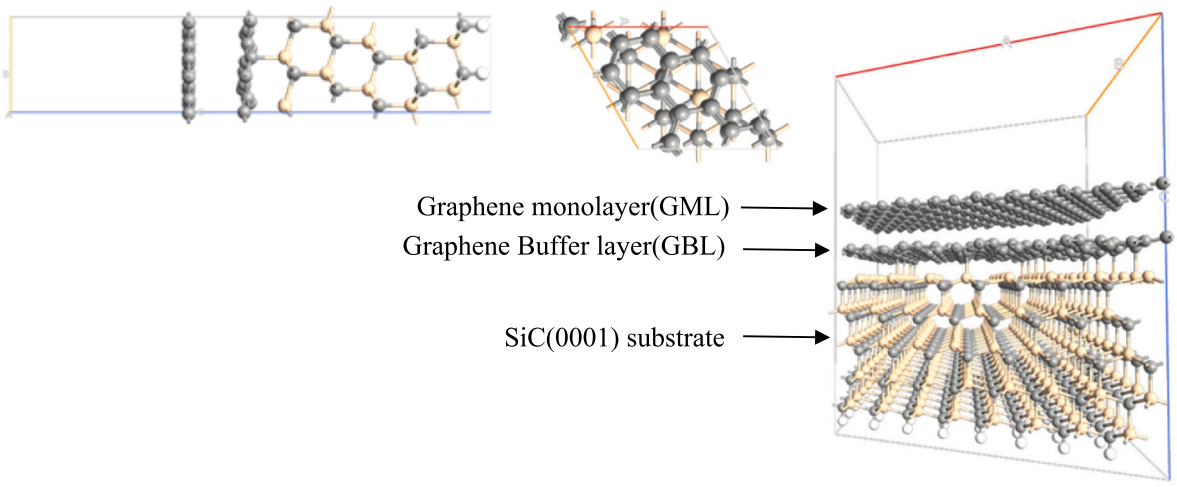


Fig. 1. The ball and stick representation of the GML@GBL@SiC (0001) after the optimization; the grey-dark, gold and white sticks are the C, Si and H atoms, respectively. (For interpretation of the references to colour in this figure legend, the reader is referred to the web version of this article.)

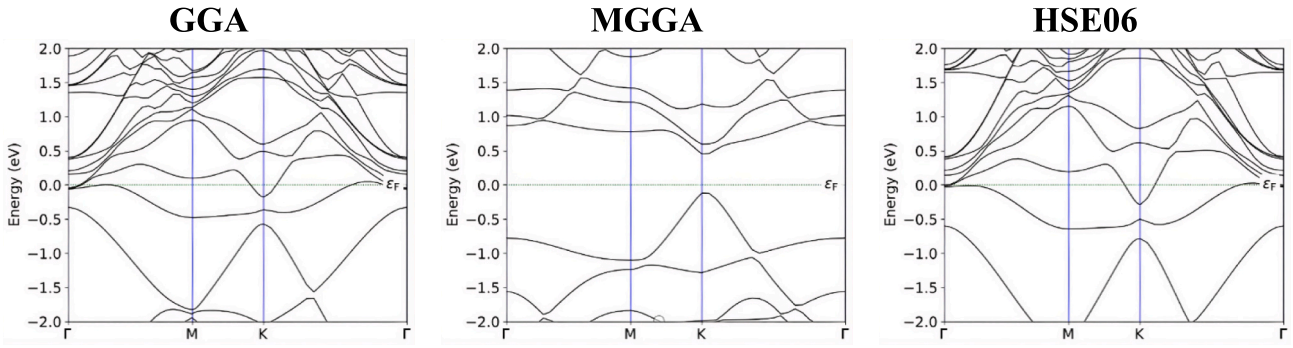


Fig. 2. Band structure of GML on SiC (0001) surface, along the high symmetry directions in their first Brillouin zone; Fermi energy has set to be zero.

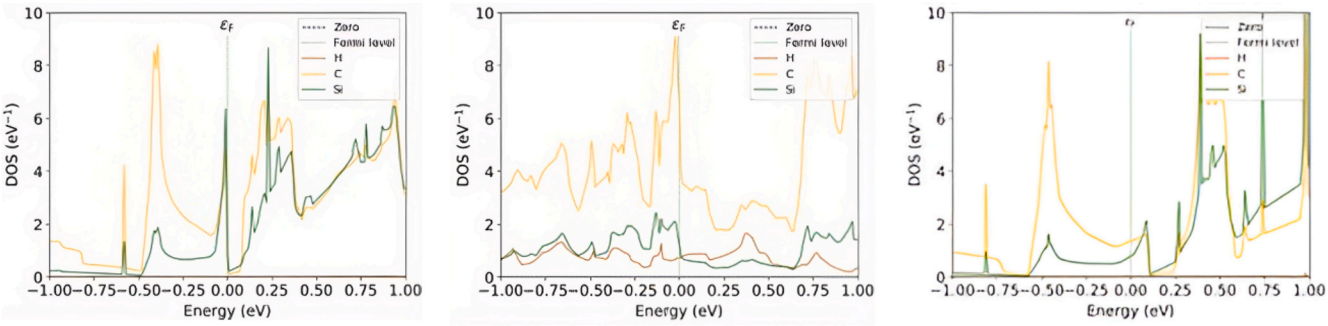


Fig. 3. DOS calculations of GML on SiC (0001) surface, Si, C and H PDOS are coloured in green, yellow and orange solid lines, respectively. (For interpretation of the references to colour in this figure legend, the reader is referred to the web version of this article.)

gaps, its performance on mixed-dimensionality interfaces such as semi-metallic 2D graphene on a 3D polar semiconductor like SiC is highly sensitive to the local dielectric screening environment, which may over- or under-estimate non-local screening depending on the exact interface separation and structural relaxation. In this specific configuration, the combination of relaxed interface geometry and screening physics under HSE06 favours a metallic crossing, missing the subtle potential perturbation that the MGGA is highly sensitive to via the τ(r).

The HOMO-LUMO band gap and eigenstate energy levels of GML over the substrate calculated with various functionals, are shown in Fig. 4. The HOMO-LUMO gap has been predicted to be 3.44 eV, 2.43 eV, and 4.57 eV by the GGA, MGGA, and HSE06, respectively. The eigenstate variation in the region below the Fermi energy, as determined by the data from DFT calculations, suggests that the Molecular Orbitals (MOs) for MGGA are shifting toward higher/lower energies for HOMO/LUMO; that is, the HOMO energy value has changed from −1.5648 for MGGA to −2.0924 eV for GGA and − 2.7871 eV for HSE06. Remarkably, the LUMO state's energy level has risen from 0.8650 eV for MGGA to 1.3513 eV for GGA and 1.7796 eV for HSE. The results of the HOMO-LUMO isosurfaces show that while the LUMO state displays the electron orbitals spreading over the GBL and the Si atoms in the substrate, the HOMO calculated by MGGA is delocalized over all the C in GBL, Si *p* orbitals, and some C atoms in GML lattice. The electron density redistribution in the HOMO state shows that charge removal from the

Table 1
Electronic band gap of GML on the SiC (0001) surface obtained with different functionals in our study, has compared to other experimental and theoretical references.

	Band gap (eV)
This study (GGA/PBE)	0.00
This study (MGGA/TB09)	0.57
This study (HSE06)	0.00
Exp. Zhou et al. [27]	0.26
Exp. Sugawara et al. [29]	0.25
Exp. Coletti et al. [28]	0.25–0.31
DFT. Mattausch et al. [31](GGA/LDA)	0.00
DFT. Peng et al. [30](GGA/PBE)	0.00

graphene sheets, specifically from the π-electron system in GBL. In the other part, the HOMO state of the interface calculated by GGA indicated electron density channels between GBL and SiC atoms (they are acting as electron donors). The corresponding LUMO appears as fully delocalized MOs throughout all the interfaces, including the GML atoms. Furthermore, the HOMO state of the total interface predicted by HSE06 is similar to GGA one with a lower energy position; however, the charge density has only redistributed on GBL and the first atom surface of SiC (0001) and GML did not participated in the electron density delocalization.

Regarding to the orbital localization and functional dependence, our isosurface results in Fig. 4 reveal that orbital localization is highly sensitive to the choice of each functional, which fundamentally stems from how they handle electron self-interaction errors. The MGGA functional predicts a narrower band gap (2.43) eV with the HOMO fully delocalized over the GBL, Si *p* orbitals, and parts of the GML. The LUMO spreads across the GBL and substrate Si atoms. This indicates a high degree of spatial overlap. The GGA/PBE functional yields a moderate gap (3.44 eV). The HOMO shifts downward to −2.0924 eV, showing a localized redistribution that forms distinct electron density channels specifically between the GBL and SiC atoms. The hybrid HSE06 functional corrects for self-interaction errors, shifting the HOMO further down to −2.7871 eV and widening the gap to 4.57 eV. Here, the HOMO charge density localizes strictly on the GBL and the topmost SiC surface layer, leaving the GML completely out of the delocalization.

The spatial distribution of the MOs directly reflects the nature of the interface hybridization between the graphene layers and the SiC(0001) substrate. Both GGA and HSE show strong hybridization between the GBL and the first atomic layer of the SiC substrate. The presence of "electron density channels" in GGA and the localized redistribution in HSE06 confirm chemical interaction and charge restructuring at this specific sub-interface. In the HSE06 description, the GML does not participate in the HOMO delocalization. This suggests that the GBL effectively screens the top GML from direct hybridization with the substrate, preserving the intrinsic electronic properties of the outermost graphene layer. More, the charge removal from the GBL π-system indicates that the interface acts as an electron donor system, driving a strategic redistribution of carrier density. According to the influence of any DFT functional on charge transport in GML@SiC interface, the structural localization and hybridization directly indictate the expected charge transport behavior across the heterostructure. The electron density channels identified by GGA between the GBL and SiC facilitate vertical charge tunneling across the interface. Further, since the HSE06 functional shows that the GML does not participate in the interface HOMO delocalization, lateral charge transport within the GML is expected to suffer minimal scattering from substrate defects. Indeed, MGGA suggests a highly delocalized system that would imply lower resistance across all layers.

As is well known, in the graphene monolayer, the charge carriers have zero m^* momentum close to the Dirac points, where the electron energy-momentum relationship is linear. These particles have a constant effective velocity and behave similarly to relativistic Dirac fermions. In this study, as displayed in Table 2, the m^* values are the electron effective mass have predicted for GML on SiC substrate determined for the bands index before and after the Fermi energy. As seen in this **Table**, along the K line in reciprocal space, the higher m^* value near to VBL for GML@SiC(0001) has predicted by MGGA with 1.162 m_e. The lower values of −0.569 m_e/0.234 m_e have calculated by GGA/HSE06 functional, respectively. It is worthy to notice that an electron with a negative effective mass will accelerate in the opposite direction of the applied force (e.g., it moves backward when pushed forward) and has a negative symbol. So, in the absence of the electron, the hole positioned in a nearly full valence band. Changing the m^* shows a similar tendency to what we observed in the band structure calculations and HOMO-LUMO band gaps. Since in the GML@SiC(0001) interface calculated by the GGA and HSE06 functional, there is no electronic band gap and HOMO-LUMO states are transferred far from the Fermi level (shifted to higher energies), this can lead to negative m^* for the electron and the presence of the holes near to VBL. In comparison, the same system computed by MGGA generally has positive m^* energies for electrons than holes with an open band gap and lower HOMO-LUMO energy states.

Then, we simulated the optical properties of the *Re*(*ω*) and *Im(ω)* parts of the dielectric constant $\sigma(\omega)$, n and κ parameters of the GML monolayer over the adsorption on SiC (0001) (Fig. 5). In comparison, we applied three GGA, MGGA, and HSE06 functionals, and the calculations were done along the *xx*-, *yy*- (in-plane), and *zz*-direction (out-of-plane) polarizations.

Based on DFT calculations using different methodologies, the results related to the *Re*(*ω*) and *Im(ω)* parts (Fig. 5) may clearly show the difference in optical properties. The first optical peak from the *Im(ω)* of the dielectric constant is approximately 36 THz, with varying intensities of 8.60, 16.60, and 1.48 calculated with GGA, MGGA, and HSE06 along the *xx* in-plane direction. Moreover, the optical spectra associated with the MGGA calculation show a peak around 48 THz with an intensity of 8.35 along the *yy* in-plane direction. Along the zz-direction calculated by all the functionals, the *Re*(*ω*) indicated lower values. Moreover, *Re*(*ω*) of GML has been calculated by MGGA are remarkably high as 28.03, 18.76, and 2.15 along with the *xx*-, *yy*-, and *zz*- out-of-plane polarizations, respectively. The corresponding values calculated by GGA and HSE06 are roughly 20.8 and 6.50, respectively.

The *Re*(*ω*) and the *Im(ω)* parts of the dielectric constant of GML@SiC (0001) with respect to GBL@SiC(0001), showed that the first optical spectra in the *Im(ω)* part of the dielectric constant are estimated to be 181 THz based on the DFT work of Mohebbi et al. [7]. According to this study, Re(ω) was determined to be 2.34, 2.32, and 1.07 for GBL over the SiC (0001) along with the *xx*-, *yy*-, and *zz*- out-of-plane polarizations, respectively. While the experimental measurements made by Santos et al. [71,72] and Hong et al. [72] have reported the *Re*(*ω*) values around 1.8–3 for the pure graphene monolayer, the atomistic study done by Ostovari et al. [73] predicted the *Re*(*ω*) of 2.6 and 1.4 along the in-plane and out-of-plane polarizations, respectively. A comparison between our optical results with the previous works reveals that *Re*(*ω*) of graphene has significantly increased along in-plane directions when GML interacts with the SiC substrate, and *Im(ω)* first peaks have shifted to the THz non-zero lower frequencies.

According to Fig. 5, the $\sigma(\omega)$ approximated values by GGA, MGGA and HSE06 are 778 AV^{-1} cm^{-1}, 635 AV^{-1} cm^{-1} and 773 AV^{-1} cm^{-1} at 139 THz, 72 THz, and 205 THz for GML@SiC along the in-plane directions, respectively. While the spectrum calculated by GGA and HSE06 indicated the same values along the *yy*- in-plane direction, the one related to MGGA shows another peak around 157 THz with intensity 1093 AV^{-1} cm^{-1}. The static values n calculated by the MGGA functional for GML along the *xx*-, *yy*- in-plane and *zz*- out-of-plane polarization directions are 5.29, 4.33, and 1.46, respectively, compared to the lower values of 4.54/1.57 (GGA) and 2.55/1.19 (HSE06) along the in-plane/out-of-plane directions, respectively. More, the maximum initial non-zero values of κ are about 36 THz, 72 THz, and 48 THZ computed by

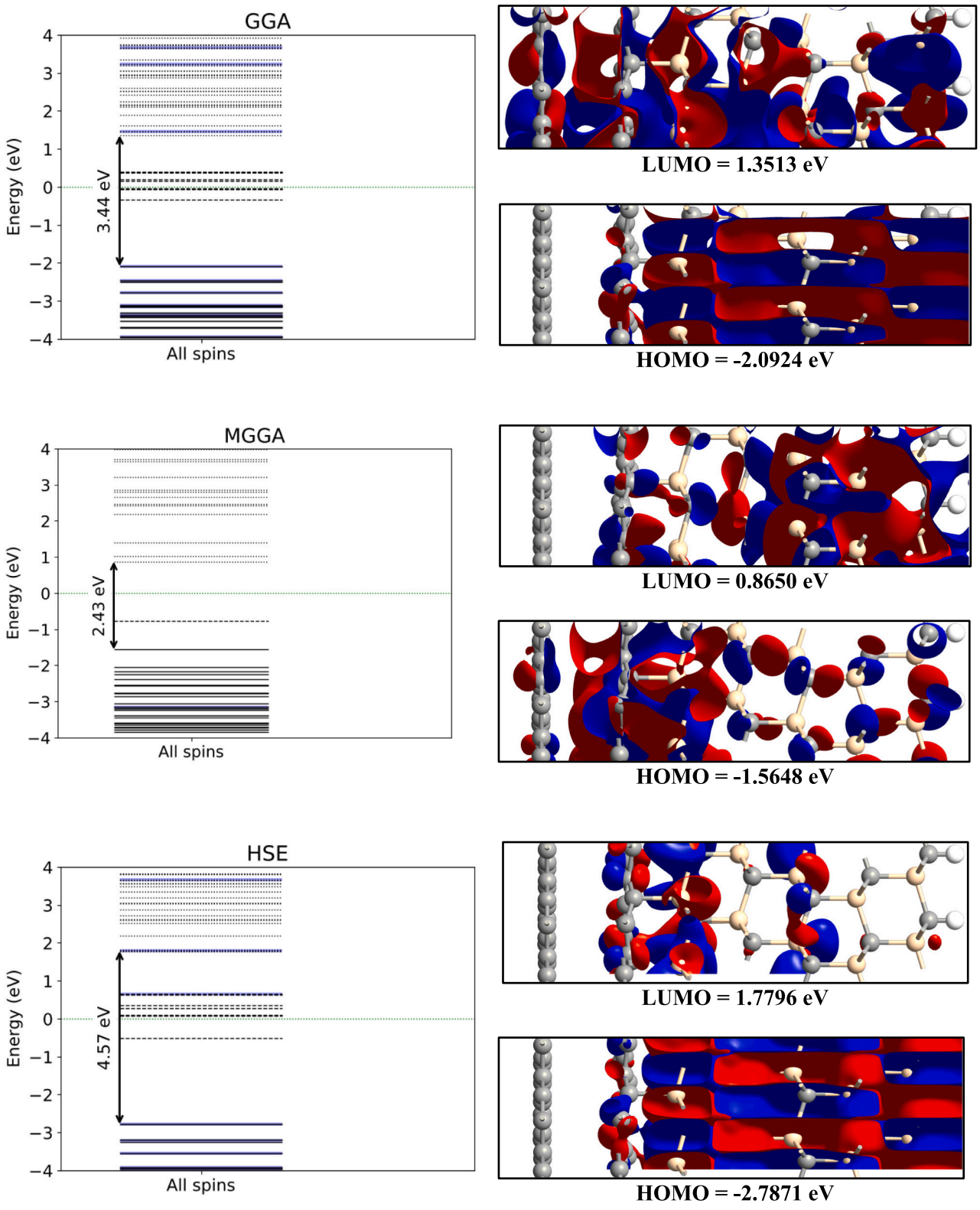


Fig. 4. Molecular Energy Spectrum and HOMO-LUMO isosurfaces of GML on SiC (0001) surface.

Table 2
The m^* along the K in reciprocal space calculated by different methodology.

	GGA	MGGA	HSE06
m^* near to CBL	0.454 m_e	0.476 m_e	0.222 m_e
m^* near to VBL	−0.569 m_e	1.162 m_e	−0.234 m_e

GGA, MGGA, and HSE06 for GML@SiC(0001).

4. Conclusion

To investigate the electronic and optical characteristics of GML on SiC(0001) substrate, three distinct GGA, MGGA, and HSE06 functionals

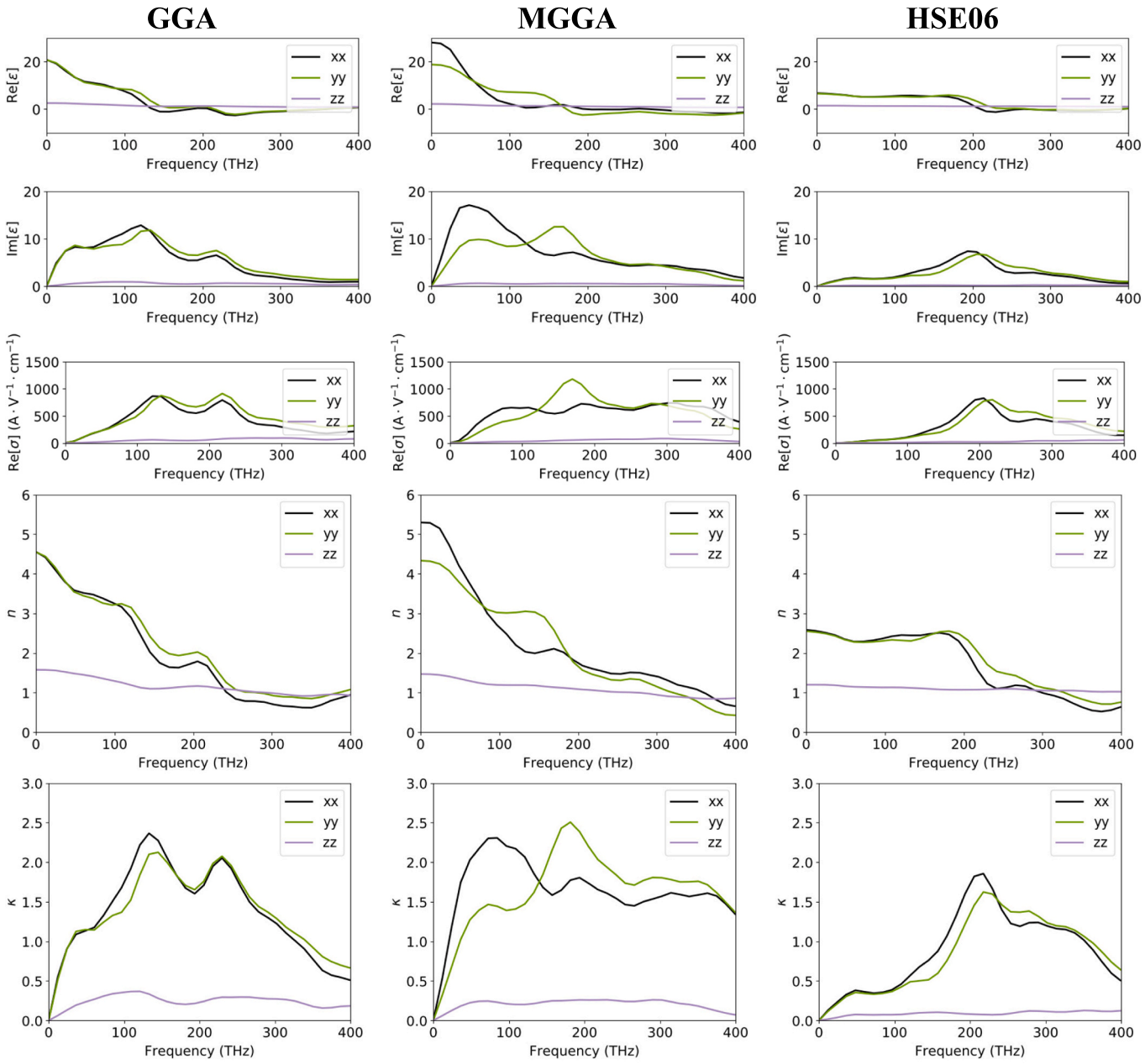


Fig. 5. The *Re*(*ω*) and *Im*(*ω*), $\sigma(\omega)$, n and κ of GML on SiC(0001) at THz frequencies.

have been employed. Following the full optimization of the supercell, the band structure calculations have been assessed. The MGGA functional, for the first time, has yielded a direct band gap of 0.57 eV in agreement to the experimental measurements which showed that GML@SiC(0001) is semiconductor. The metallic characteristics of this interface have been predicted by GGA and HSE06 functionals. Along the K line in reciprocal space for the GML@SiC(0001) interface, the m^* values of 1.162 m_e /0.476 m_e, −0.569 m_e/0.454 m_e, and − 0.234 m_e /0.222 m_e have calculated by MGGA, GGA, and HSE functional, respectively. Calculated data using GGA, MGGA, and HSE06 along the *xx* in-plane direction reveal that the first optical peak from the Im(ω) is roughly 36 THz, while the optical spectra linked to the MGGA computation display a peak along the *yy* in-plane direction at around 48 THz with an intensity of 8.35. Additionally, the in-plane polarizations and Re (ω) of GML, as determined by GGA, MGGA, and HSE06, are exceptionally high at 20.8, 28.03, and 6.50, respectively.

In summary, this study clarifies the critical role of functional choice in predicting the electronic properties of heterogeneous GML@SiC (0001) interface. The reasons why the GGA, MGGA, and HSE06 functionals show these specific electronic trends at the GML/SiC interface are directly addressed to the physics of self-interaction error, τ(r), and dielectric screening. Specifically, GGA/PBE over-delocalizes electronic states across the interface, leading to an incorrect prediction of purely metallic behavior of this interface. In contrast, the MGGA functional—by utilizing the τ(r) —successfully recognizes variations in electron localization topologies. This partially mitigates self-interaction errors and resolves the symmetry-breaking effects induced by the SiC substrate, correctly opening a small electronic band gap. Meanwhile, the performance of the HSE06 hybrid functional is highly sensitive to the local dielectric screening environment of mixed-dimensionality interfaces, where the specific structural relaxation favours a metallic crossing.

Beyond the scope of computational methodology, these findings possess broader scientific significance for the design and engineering of

next-generation 2D/3D electronic devices. In details, the first point is related to the Predictive Materials Design, since the reported results establish a rigorous physics-based framework for interpreting electronic transport at mixed-dimensionality interfaces. More, local density gradients and screening environment drastically alter band gap opening allows researchers to reliably model and predict the behaviours of other 2D/3D systems (e.g., graphene on GaN or transition metal dichalcogenides on oxides). The second point is related to the Device Application Insights. The discovery that substrate-induced symmetry breaking can open a small, tunable band gap under proper electronic description (MGGA) provides critical guidelines for engineering graphene-based field-effect transistors (FETs), where controlled band-gap opening is essential for achieving acceptable on/off current ratios. The third and final point is related to the Interfacial Engineering. In detail, the sensitivity of HSE06 to the local screening environment highlights that subtle experimental variations in interface separation or structural relaxation can switch the band gap properties. This suggests that mechanical strain or dielectric encapsulation can be actively used as tuning forks to manipulate Schottky barrier heights and contact resistances in 2D/3D device architectures.

Author contribution

Author Contributions: Conceptualization, E.M., E.L. and P.S.; methodology, E.M. and E.L.; validation, E.M., E.L., P.S., L.P., and D.M; investigation, E.M.; data curation, E.M.; writing—original draft preparation, E.M.; writing—review and editing, E.M., E.L., E.P., P.S., M.P., L. P., and D.M.; visualization, E.M.; supervision, P.S.; project administration, E.M., E.L., E.P., P.S., L.P. and D.M. All authors have read and agreed to the published version of the manuscript.

CRediT authorship contribution statement

Elaheh Mohebbi: Writing – review & editing, Writing – original draft, Visualization, Project administration, Methodology, Investigation, Data curation, Conceptualization. **Pierluigi Stipa:** Writing – review & editing, Validation, Supervision, Project administration, Conceptualization. **Eleonora Pavoni:** Writing – review & editing, Project administration. **Marina Petroselli:** Writing – review & editing. **Luca Pierantoni:** Writing – review & editing, Validation, Project administration. **Emiliano Laudadio:** Writing – review & editing, Validation, Project administration, Methodology, Conceptualization. **Davide Mencarelli:** Writing – review & editing, Validation, Project administration.

Declaration of competing interest

The authors declare that they have no known competing financial interests or personal relationships that could have appeared to influence the work reported in this paper.

Acknowledgment

This work is part of the research of HORIZON-EIC-2022-PATHFINDEROPEN-01 “Nano-scale Development of Plasmonic Amplifiers Based on 2D Materials” (PLASNANO) (grant agreement No. 101099552).

Data availability

No data was used for the research described in the article.

References

[1] Z.R. Robinson, G.G. Jernigan, K.M. Bussmann, L.O. Nyakiti, N.Y. Garces, A. Nath, V.D. Wheeler, R.L. Myers-Ward, D.K. Gaskill, C.R. Eddy Jr., Graphene growth on SiC (000−1): Optimization of surface preparation and growth conditions, Carbon Nanotubes, Graphene, and Emerging 2D Materials for Electronic and Photonic Devices VIII, SPIE, 2015, pp. 70–76.
[2] W. Norimatsu, M. Kusunoki, Epitaxial graphene on SiC {0001}: advances and perspectives, Phys. Chem. Chem. Phys. 16 (2014) 3501–3511.
[3] L. Nemec, F. Lazarevic, P. Rinke, M. Scheffler, V. Blum, Why graphene growth is very different on the C face than on the Si face of SiC: insights from surface equilibria and the (3× 3)-3 C-SiC (1^{-} 1^{-} 1^{-}) reconstruction, Phys. Rev. B 91 (2015) 161408.
[4] W. Norimatsu, M. Kusunoki, Epitaxial graphene on SiC {0001}: advances and perspectives, Phys. Chem. Chem. Phys. 16 (2014) 3501–3511.
[5] Y. Qi, S.H. Rhim, G.F. Sun, M. Weinert, L. Li, Epitaxial graphene on SiC (0001): more than just honeycombs, Phys. Rev. Lett. 105 (2010) 085502.
[6] S. Gad, E.M. Gad, H.F. Khalil, Graphene beyond limits: Progress in properties, applications, in: Graphene-The Next Generation Material: The Next Generation Material 1, 2025.
[7] P. Kumar, A.K. Singh, S. Hussain, K.N. Hui, K. San Hui, J. Eom, J. Jung, J. Singh, Graphene: synthesis, properties and application in transparent electronic devices, Rev. Adv. Sci. Eng. 2 (2013) 238–258.
[8] A. Ibrahim, A. Klopocinska, K. Horvat, Z. Abdel Hamid, Graphene-based nanocomposites: synthesis, mechanical properties, and characterizations, Polymers 13 (2021) 2869.
[9] S.P. Vinodhini, J.R. Xavier, Recent progress in graphene-based nanocomposites for enhanced energy storage and corrosion protection, J. Mater. Sci. 60 (2025) 14837–14879.
[10] N.O. Weiss, H. Zhou, L. Liao, Y. Liu, S. Jiang, Y. Huang, X. Duan, Graphene: an emerging electronic material, Adv. Mater. 24 (2012) 5782–5825.
[11] S.K. Pandey, A. Mohammad, R.K. Singh, Graphene: Properties and Applications, in: Next-Generation Nanomaterials for Sustainable Engineering, Springer, 2026, pp. 51–71.
[12] T.T. Tung, M.J. Nine, M. Krebsz, T. Pasinszki, C.J. Coghlan, D.N.H. Tran, D. Losic, Recent advances in sensing applications of graphene assemblies and their composites, Adv. Funct. Mater. 27 (2017) 1702891.
[13] M. Haqgu, Z. Rostami, A. Mengboev, DFT investigation of aflatoxin B1 adsorption on vacancy-defective graphene: electronic properties and sensing potential, Chem. Rev. Lett. 8 (2025) 1258–1268.
[14] S.J. Hoseyni, A. Karbakhshzadeh, A. Moshtaghi Zonouz, B. Husseen, Computational investigation on interaction between graphene nanostructure BC3 and antiparkinson drug amantadine: possible sensing study of BC3 and its doped derivatives on amantadine, Chem. Rev. Lett. 7 (2024) 380–387.
[15] M.R. Poor Heravi, B. Azizi, E. Abdulkareem Mahmood, A.G. Ebadi, M.J. Ansari, S. Soleimani-Amiri, Molecular simulation of the paracetamol drug interaction with Pt-decorated BC3 graphene-like nanosheet, Mol. Simul. 48 (2022) 517–525.
[16] Z.H. Hussein, F.F. Karam, N. Rahi Mashkur, Thermodynamic, kinetic studies and adsorption conditions for removal of dye from aqueous solution using reduced graphene oxide (RGO), Chem. Rev. Lett. 8 (2025) 128–136.
[17] S. Esfahani, J. Akbari, S. Soleimani-Amiri, M. Mirzaei, A.G. Gol, Assessing the drug delivery of ibuprofen by the assistance of metal-doped graphenes: insights from density functional theory, Diam. Relat. Mater. 135 (2023) 109893.
[18] S. Esfahani, J. Akbari, S. Soleimani-Amiri, Adsorption of ibuprofen by an iron-doped silicon carbide graphene monolayer: DFT exploration of drug delivery insights, Int. J. Nano Dimens. 15 (2024).
[19] R. Behjatmanesh-Ardakani, R. Rzayev, Pd-and Pt-doped graphene quantum dots for SO2 adsorption and dissociation: a non-periodic DFT study, Chem. Rev. Lett. 7 (2024) 1022–1030.
[20] B.F. Machado, P. Serp, Graphene-based materials for catalysis, Catal, Sci. Technol. 2 (2011) 54–75.
[21] R. Behjatmanesh-Ardakani, R. Rzayev, Hydrogen assisted SO2 dissociation on the Pt-doped graphene quantum dot surface: a non-periodic DFT study, Chem. Rev. Lett. 8 (2025) 178–186.
[22] E. Vessally, S. Soleimani-Amiri, A. Hosseinian, L. Edjlali, A. Bekhradnia, A comparative computational study on the BN ring doped nanographenes, Appl. Surf. Sci. 396 (2017) 740–745.
[23] J. Liu, C. Wang, T. Liang, W. Lai, Density functional theory investigation of oxygen interaction with boron-doped graphite, Appl. Surf. Sci. 390 (2016) 273–282.
[24] A.A. Peyghan, M. Noei, M.B. Tabar, A large gap opening of graphene induced by the adsorption of co on the Al-doped site, J. Mol. Model. 19 (2013) 3007–3014.
[25] M.S. Nevius, M. Conrad, F. Wang, A. Celis, M.N. Nair, A. Taleb-Ibrahimi, A. Tejeda, E.H. Conrad, Semiconducting graphene from highly ordered substrate interactions, Phys. Rev. Lett. 115 (2015) 136802.
[26] E. Mohebbi, E. Pavoni, P. Stipa, M. Petroselli, L. Pierantoni, E. Laudadio, D. Mencarelli, Reliable prediction of the band gap properties of graphene buffer layer on SiC using meta-GGA approximation, Carbon Trends. 21 (2025) 100575.
[27] S.Y. Zhou, G.-H. Gweon, A.V. Fedorov, P.N. First de, W.A. De Heer, D.-H. Lee, F. Guinea, A.H. Castro Neto, A. Lanzara, Substrate-induced bandgap opening in epitaxial graphene, Nat. Mater. 6 (2007) 770–775.
[28] C. Coletti, C. Riedl, D.S. Lee, B. Krauss, L. Patthey, K. von Klitzing, J.H. Smet, U. Starke, Charge neutrality and band-gap tuning of epitaxial graphene on SiC by molecular doping, Phys. Rev. B Condens. Matter Mater. Phys. 81 (2010) 235401.
[29] K. Sugawara, K. Suzuki, M. Sato, T. Sato, T. Takahashi, Enhancement of band gap and evolution of in-gap states in hydrogen-adsorbed monolayer graphene on SiC (0001), Carbon 124 (2017) 584–587.
[30] X. Peng, R. Ahuja, Symmetry breaking induced bandgap in epitaxial graphene layers on SiC, Nano Lett. 8 (2008) 4464–4468.
[31] A. Mattausch, O. Pankratov, Ab initio study of graphene on SiC, Phys. Rev. Lett. 99 (2007) 076802.

[32] T. Cavallucci, V. Tozzini, Multistable rippling of graphene on SiC: a density functional theory study, J. Phys. Chem. C 120 (2016) 7670–7677.
[33] N.M. Caffrey, R. Armiento, R. Yakimova, I.A. Abrikosov, Changes in work function due to NO 2 adsorption on monolayer and bilayer epitaxial graphene on SiC (0001), Phys. Rev. B 94 (2016) 205411.
[34] S. Kopylov, A. Tzalenchuk, S. Kubatkin, V.I. Fal'ko, Charge transfer between epitaxial graphene and silicon carbide, Appl. Phys. Lett. 97 (2010).
[35] A. Mattausch, O. Pankratov, Ab initio study of graphene on SiC, Phys. Rev. Lett. 99 (2007) 076802.
[36] K. Liu, P. Yan, J. Li, C. He, T. Ouyang, C. Zhang, C. Tang, J. Zhong, Effect of hydrogen passivation on the decoupling of graphene on SiC (0001) substrate: first-principles calculations, Sci. Rep. 7 (2017) 8461.
[37] J. Guse, S. Wundrack, M. Eckert, P. Richter, S. Wolff, N. Tilgner, P. Schädlich, M. Gruschwitz, K. Küster, B. Harling, Growth dynamics of graphene buffer layer formation on ultra-smooth SiC (0001) surfaces, ArXiv Preprint ArXiv.1 (2025) 2503.01757.
[38] P.D. Bentley, T.W. Bird, A.P.J. Graham, O. Fossberg, S.P. Tear, A. Pratt, Formation of quasi-free-standing graphene on SiC (0001) through intercalation of erbium, AIP Adv. 11 (2021).
[39] M.L. Ackerman, P. Kumar, M. Neek-Amal, P.M. Thibado, F.M. Peeters, S. Singh, Anomalous dynamical behavior of freestanding graphene membranes, Phys. Rev. Lett. 117 (2016) 126801.
[40] K. Qiao, Y. Liu, C. Kim, R.J. Molnar, T. Osadchy, W. Li, X. Sun, H. Li, R.L. Myers-Ward, D. Lee, Graphene buffer layer on SiC as a release layer for high-quality freestanding semiconductor membranes, Nano Lett. 21 (2021) 4013–4020.
[41] M. Beshkova, L. Hultman, R. Yakimova, Device applications of epitaxial graphene on silicon carbide, Vacuum 128 (2016) 186–197.
[42] E. Mohebbi, E. Pavoni, P. Stipa, M. Petroselli, C. Minnelli, L. Pierantoni, D. Mencarelli, M. Aldrigo, E. Laudadio, M.M.S. Fakhrabadi, Electronic structure of 1, 4-Phenylenediacrylic acid on graphene and bilayer graphite: from experiments to DFT and ab initio molecular dynamics simulations, Chem. Phys. Impact 11 (2025) 100947.
[43] E. Mohebbi, E. Pavoni, L. Pierantoni, P. Stipa, A. Hemmetter, E. Laudadio, D. Mencarelli, Towards graphene-based asymmetric diodes: a density functional tight-binding study, Nanoscale Adv 6 (2024) 1548.
[44] E. Mohebbi, E. Pavoni, L. Pierantoni, P. stipa, E. Laudadio, D. Mencarelli, Insights Into a New Geometric Graphene Diode with Ultrahigh Asymmetry Ratio: A Computational Approach, 2023 IEEE 23rd international conference on nanotechnology (NANO), IEEE, 2023, pp. 238–242.
[45] S. Smidstrup, T. Markussen, P. Vancraeyveld, J. Wellendorff, J. Schneider, T. Gunst, B. Verstichel, D. Stradi, P.A. Khomyakov, U.G. Vej-Hansen, QuantumATK: an integrated platform of electronic and atomic-scale modelling tools, J. Phys. Condens. Matter 32 (2019) 015901.
[46] W. Kohn, L.J. Sham, Self-consistent equations including exchange and correlation effects, Phys. Rev. 140 (1965) A1133.
[47] M. Ernzerhof, G.E. Scuseria, Perspective on "Inhomogeneous electron gas" Hohenberg P, Kohn W (1964) Phys rev 136: B864, Theor. Chem. Accounts 103 (2000) 259–262.
[48] E. Laudadio, E. Mohebbi, E. Pavoni, C. Minnelli, S. Sabbatini, P. Stipa, Density functional theory and molecular dynamics studies on electrical, mechanical, and thermal properties of TiO2 nanoparticles interacting with poly lactic-co-glycolic acid, Colloids Surf. A Physicochem. Eng. Asp. 667 (2023) 131388.
[49] D. Sánchez-Portal, P. Ordejon, E. Artacho, J.M. Soler, Density-functional method for very large systems with LCAO basis sets, Int. J. Quantum Chem. 65 (1997) 453–461.
[50] C.J. Schattenberg, A. Wodynski, H. Åström, D. Sundholm, M. Kaupp, S. Lehtola, Revisiting gauge-independent kinetic energy densities in Meta-GGAs and local hybrid calculations of Magnetizabilities, J. Phys. Chem. A 127 (2023) 10896–10907.
[51] F. Tran, P. Kovács, L. Kalantari, G.K.H. Madsen, P. Blaha, Orbital-free approximations to the kinetic-energy density in exchange-correlation MGGA functionals: tests on solids, J. Chem. Phys. 149 (2018).
[52] J. Heyd, G.E. Scuseria, Efficient hybrid density functional calculations in solids: assessment of the Heyd–Scuseria–Ernzerhof screened coulomb hybrid functional, J. Chem. Phys. 121 (2004) 1187–1192.
[53] Z. Wan, Q. De Wang, D. Liu, J. Liang, Effectively improving the accuracy of PBE functional in calculating the solid band gap via machine learning, Comput. Mater. Sci. 198 (2021), https://doi.org/10.1016/j.commatsci.2021.110699.
[54] J. Tao, J.P. Perdew, V.N. Staroverov, G.E. Scuseria, Climbing the density functional ladder: nonempirical meta–generalized gradient approximation designed for molecules and solids, Phys. Rev. Lett. 91 (2003) 146401.
[55] M. Ernzerhof, G.E. Scuseria, Assessment of the Perdew–burke–Ernzerhof exchange-correlation functional, J. Chem. Phys. 110 (1999) 5029–5036.
[56] E. Mohebbi, M.M.S. Fakhrabadi, Electronic, optical, mechanical, and thermal properties of diphenylacetylene-based graphyne nanosheet using density functional theory, Nanotechnology 32 (2021) 405705.
[57] E. Mohebbi, E. Pavoni, L. Pierantoni, P. Stipa, G.M. Zampa, E. Laudadio, D. Mencarelli, Band gap and THz optical adsorption of SnSe and SnSe2 nanosheets on graphene: negative dielectric constant of SnSe, Results Phys 57 (2024) 107415.
[58] A. Patra, B. Patra, L.A. Constantin, P. Samal, Electronic band structure of layers within meta generalized gradient approximation of density functionals, Phys. Rev. B 102 (2020) 045135.
[59] S. Luo, Y. Zhao, D.G. Truhlar, Improved CO Adsorption Energies, Site Preferences, and Surface Formation Energies from a Meta-Generalized Gradient Approximation Exchange–Correlation Functional, M06-L, J. Phys. Chem. Lett. 3 (2012) 2975–2979.
[60] Y. Duan, L. Qin, L. Shi, G. Tang, More accurate predictions of band gap tuned by pressure in InN using HSE06 and GW approximations, Comput. Mater. Sci. 101 (2015) 56–61.
[61] E. Mohebbi, E. Pavoni, D. Mencarelli, P. Stipa, L. Pierantoni, E. Laudadio, PBEsol/HSE functional: a promising candidate for vanadium dioxide (B) characterization, RSC Adv. 12 (2022) 31255–31263.
[62] S. Ehrlich, J. Moellmann, W. Reckien, T. Bredow, S. Grimme, System-dependent dispersion coefficients for the DFT-D3 treatment of adsorption processes on ionic surfaces, ChemPhysChem 12 (2011) 3414–3420.
[63] P.A. Denis, C.P. Huelmo, F. Iribarne, On the band gaps and effective masses of mono and dual doped monolayer graphene, Comput. Mater. Sci. 137 (2017) 20–29.
[64] M.P. Desjarlais, Density functional calculations of the reflectivity of shocked xenon with ionization based gap corrections, contributions to, Plasma Phys. 45 (2005) 300–304.
[65] J.E. Sipe, E. Ghahramani, Nonlinear optical response of semiconductors in the independent-particle approximation, Phys. Rev. B 48 (1993) 11705.
[66] E. Mohebbi, E. Pavoni, P. Stipa, L. Pierantoni, E. Laudadio, D. Mencarelli, Tunable optical properties of cu/VSe2 from the visible to terahertz spectral range: a first-principles study, Int. J. Mol. Sci. 26 (2025) 2527.
[67] P. Mårtensson, F. Owman, L.I. Johansson, Morphology, atomic and electronic structure of 6H-SiC (0001) surfaces, Phys. Status Solidi B 202 (1997) 501–528.
[68] L. Li, I.S.T. Tsong, Atomic structures of 6H SiC (0001) and (0001¯) surfaces, Surf. Sci. 351 (1996) 141–148.
[69] S. Goler, C. Coletti, V. Piazza, P. Pingue, F. Colangelo, V. Pellegrini, K.V. Emtsev, S. Forti, U. Starke, F. Beltram, Revealing the atomic structure of the buffer layer between SiC (0001) and epitaxial graphene, Carbon N. Y. 51 (2013) 249–254.
[70] L. Bellucci, T. Cavallucci, V. Tozzini, From the buffer layer to graphene on silicon carbide: exploring morphologies by computer modeling, Front. Mater. 6 (2019) 198.
[71] E.J.G. Santos, E. Kaxiras, Electric-field dependence of the effective dielectric constant in graphene, Nano Lett. 13 (2013) 898–902.
[72] X. Hong, W. Yu, D.D.L. Chung, Electric permittivity of reduced graphite oxide, Carbon N. Y. 111 (2017) 182–190.
[73] F. Ostovari, M. Hasanpoori, M. Abbasnejad, M.A. Salehi, DFT calculations of graphene monolayer in presence of Fe dopant and vacancy, Phys. B Condens. Matter 541 (2018) 6–13.